JOURNAL OF SOLID STATE CHEMISTRY 96, 84–96 (1992)

Structural and Magnetic Properties of Some AgF^+ Salts*

WILLIAM J. CASTEEL, JR., GEORGE LUCIER, RIKA HAGIWARA, HORST BORRMANN, AND NEIL BARTLETT

Chemical Sciences Division, Lawrence Berkeley Laboratory, and Department of Chemistry, The University of California at Berkeley, Berkeley, California 94720

Received July 29, 1991

New salts of the one-dimensional chain-cation $(Ag–F)_n^{n+}$ have been prepared, the structural and magnetic properties of which indicate that they are metallic. A single-crystal X-ray structure analysis of $AgFBF_4$ has established a linear cationic chain, the two Ag–F interatomic distances, at 296 K, being 2.002(3) and 2.009(3) Å. Magnetic susceptibility measurements on the powder from 6 to 280 K show an approximately temperature-independent paramagnetism ($\chi_M \approx 180 \times 10^{-6}$ emu mole^{-1}) with no evidence of a Peierls transition in that range. Although the previously known salt, $AgFAsF_6$, has a kinked cationic chain (with, at 166 K, Ag–F–Ag = 143.1(1)°, F–Ag–F = 175.8(1)°, Ag–F = 1.994(2) and 2.001(2) Å), it also exhibits temperature-independent paramagnetism from 280 down to 63 K, but a sharp drop in susceptibility below that temperature may signify a Peierls transition. $AgFAuF_6$, which is probably isostructural with $AgFAsF_6$, is similar to it magnetically. The salt $AgFAuF_4$ probably contains a linear cationic chain, since it is isostructural with $CuFAuF_4$, but the salt $Ag(AuF_4)_2$, like its relative $Ag(AgF_4)_2$, is a magnetically dilute paramagnet, the magnetic susceptibility of which departs very little from the Curie law between 6 and 280 K. © 1992 Academic Press, Inc.

Introduction

Recently it was discovered (*1*) that AgF^+ salts are powerful oxidizers capable of oxidizing xenon at ordinary temperatures, perfluorobutene to perfluorobutane, and perfluorobenzene to salts of $C_6F_6^+$, both of the latter at 208 K, in anhydrous hydrogen fluoride solution (*2*). These oxidations by AgF^+ imply electron transfer to the cationic Ag(II) as the first step in the reaction. This is consistent with the high second ionization potential of Ag (21.49 eV) which is the highest second ionization potential of any metal, other than the alkali metals. Indeed this suggests that the electronegativity of cationic Ag(II) in AgF^+ is akin to that of the F ligand itself. A close energetic match of the F 2*p* and the Ag 4*d* orbitals is therefore likely.

Earlier than our recent studies, Gantar *et al.* had discovered (*3*) $AgF^+AsF_6^-$ and had shown it to contain the cation as a one-dimensional chain. This salt was also formed in our studies (*4*), in the interaction of AgF_3 with AsF_5 according to the remarkable reaction

$$AgF_3 + AsF_5 \rightarrow AgFAsF_6 + \tfrac{1}{2}F_2 \quad (1)$$

in which our attempt to isolate AgF_2^+ was defeated by the elimination of elemental

* This paper is presented with warm regards and best wishes to Professor Paul Hagenmüller on the occasion of his 70th birthday.

0022-4596/92 $3.00
Copyright © 1992 by Academic Press, Inc.
All rights of reproduction in any form reserved.

fluorine. A single-crystal structure determination of $AgF^+AsF_6^-$, carried out at 186 K, has fully confirmed the earlier one of Gantar *et al.* (*3*) and shown that, at least down to 186 K, the Ag(II) in this chain is essentially equally and linearly coordinated by two F ligands (at ~2.00 Å), This and the d^9 configuration of Ag(II) implied that the chain cation should have a half-filled conduction band and be metallic.

A variety of AgF^+ salts have now been prepared and structurally characterized. They all have the weak, temperature-independent paramagnetism indicative of a partially filled band. This and other properties are in conformity with the metallic nature of the chain $(Ag–F)_n^{n+}$.

Experimental

Apparatus for preparations. All reactions were performed with a stainless steel vacuum line. Preparations were carried out in Teflon reactors assembled especially for each. The reactors were joined to the metal line via flexible fluorinated ethylene propylene (FEP) tubes and a polytetrafluoroethylene (PTFE) valve. FEP-tube reactors were prepared by first cutting lengths to ~25 cm. These tubes were softened at one end by heating in a flame, then squeezed with broad-nose pliers to seal the end. One-armed reactors consisted of one of these tubes connected directly to a PTFE valve. T-shaped reactors had two of these tubes connected to a PTFE T-joint, which itself was connected via FEP tubing to a PTFE valve. All reactors were made vacuum-tight with PTFE swage connections.

DRILAB. A Vacuum Atmospheres Corp. DRILAB containing dry argon gas was used for containment and manipulation of air-sensitive materials and vacuum-dried capillaries. Continuous monitoring of the oxygen conent of the DRILAB was accomplished with a glowing incandescent lamp filament.

X-ray powder data. The quartz capillaries used for X-ray powder diffraction studies were dried under vacuum ($<10^{-6}$ Torr) at 1070 K for 24 hr before being transferred to the DRILAB. X-ray powder samples were prepared by first loading a small quantity of material into the funnel of the capillary. A light-duty steel file was slowly drawn across the capillary, vibrating the material down toward the tip. Once ~2 cm of powder was packed into the tip of the capillary, the open end was temporarily sealed by packing with fluorocarbon grease. The capillary was removed from the DRILAB and immediately sealed by drawing down in a flame. Photographs were taken using a 45-cm-circumference G.E. camera with Straumanis loading, the radiation being Cu$K\alpha$ with a nickel filter.

Magnetic susceptibility measurements. A superconducting quantum interference device (SQUID) magnetometer with a gaseous He cooling jet was used to collect the magnetic susceptibility data. The cylindrical sample container, of length and diameter 6.5 mm, consisted of two Kel-F halves, one fitting inside the other. Inside the DRILAB, a known quantity of material was firmly packed into the smaller diameter half with a Kel-F packing tool. This was then fitted into the larger half, which had fluorocarbon grease around its inner edge for the purpose of making a gas-tight seal. The container was immediately transported to the magnetometer, where it was suspended in the He atmosphere by a thread. Both the SQUID container and the packing tool were passivated with F_2 (1500 Torr, ~3 hr) and BF_3 or AsF_5 (1500 Torr, ~6 hr) prior to use.

Materials. Cylinders of F_2, HF, and BF_3 were obtained from Matheson Gas Co., East Rutherford, NJ. Ozark–Mahoning Co. (Tulsa, OK) provided the K_2NiF_6, AgF, and AsF_5. Quartz X-ray capillaries were obtained from Charles Supper Co., Natick, MA. Chemplast Inc. (Wayne, NJ) supplied the fluorinated ethylene propylene tubing

and polytetrafluoroethylene used for reaction vessels and valves.

Freedom of the anhydrous HF (AHF) from water was ensured by condensing it (at 77 K) from the supply cylinder into a tube containing K_2NiF_6. The AHF was allowed to warm to room temperature and agitated. It was then refrozen to 77 K and evacuated to ca. 0.3 Torr. This freeze–pump–thaw cycle was repeated three or more times to remove entrapped gases.

Purification of AgF powder was accomplished by recrystallization from AHF. AgF, as supplied, was placed into one arm of a T-shaped FEP reaction vessel. Enough AHF was condensed on it at 77 K to dissolve all the AgF upon warming to room temperature. The solution obtained was decanted into the other arm of the reactor and insoluble impurities were left behind. The AHF was removed under dynamic vacuum yielding, initially, colorless $AgHF_2$ and, finally, on prolonged evacuation at ca. 0.15 Torr, yellow AgF. All other materials were used as received.

Preparations: $AgBF_4$. AgF ((1) 407 mg, 3.21 mmole; (2) 344 mg, 2.71 mmole; (3) 322 mg, 2.54 mmole) previously washed with anhydrous HF was loaded into one arm of a T-shaped FEP reactor (which had been passivated with 2 atm of F_2 for several hours, and then with 2 atm of BF_3 for several more hours just prior to use). About 3 ml of AHF was condensed, under vacuum, onto the AgF at 77 K. The AgF dissolved in the AHF on warming to room temperature. This solution was decanted into the other arm of the reactor. Then enough BF_3 was introduced into the reactor to achieve a total pressure of 1500 Torr (the vapor pressure of AHF at room temperature is 850 Torr (*5*)). Brilliantly white $AgBF_4$ immediately began to precipitate out as the reactor was vigorously agitated. More BF_3 was periodically added to replace that which was consumed in the reaction until the pressure remained constant for at least 30 min. To ensure the absence of the soluble starting material, the supernatant solution was decanted into the other arm of the reactor. The HF was then condensed back, under vacuum, at 77 K and warmed to room temperature before the solution was agitated. This decantation and back-distillation washing procedure was repeated up to seven more times. The AHF was removed under dynamic vacuum and the $AgBF_4$ vacuum-dried for about 2 hr under a dynamic vacuum of 0.1 to 0.01 Torr. The reactor was transferred to the DRILAB, where the material was manipulated in a dry argon atmosphere. X-ray powder photographs confirmed that $AgBF_4$ was the only crystalline phase (*6*).

$AgFBF_4$ (powder). In order to make the dark blue, powdered $AgFBF_4$, suitable for magnetic susceptibility and powder X-ray diffraction studies, $AgBF_4$ (795 mg, 4.08 mmole) was loaded into a one-armed FEP reactor that had been passivated as described above. AHF (~3 ml) was condensed onto the $AgBF_4$: the reactor was pressurized to 900 Torr with BF_3, and enough F_2 gas was introduced to achieve a total pressure of 1500 Torr. The solution was continuously agitated and was periodically cooled in order to dissolve more F_2 in the HF solution. After about 6 hr, when signs of F_2 uptake had ceased, the blue product was vacuum-dried as described above and removed to the DRILAB. A powder X-ray photograph was taken to assess its general purity (*1*).

$AgFBF_4$ (violet single-crystal). Violet needles, the largest of which measured about 5 mm long and 0.2 mm across, were made in a manner similar to that just described. Less $AgBF_4$ was used (52.0 mg, 0.267 mmole) in ~3 ml of AHF, and only 1000 Torr of F_2 gas and no BF_3 were maintained in the reactor. The mixture, in this instance, was not agitated, and was left undisturbed until it appeared that all of the $AgBF_4$ had been consumed. HF was re-

moved by bleeding slowly through a valve giving access to a dynamic vacuum, this slow removal being managed to avoid breakage of the fragile needles of $AgFBF_4$ by violent boiling of the HF.

$AgFBF_4$ (bronze single-crystal). The synthesis of the bronze-colored crystals was the same as the synthesis of the blue powder, with the exception of the purity of the starting material. Deliberate contamination of the solid reactant $AgBF_4$ with 5 and 10% AgF ((1) $AgBF_4$: 149.0 mg, 0.7654 mmole; AgF: 5.0 mg, 0.039 mmole; (2) $AgBF_4$: 162.1 mg, 0.8327 mmole; AgF: 11.6 mg, 0.0914 mmole) in separate experiments both resulted in bronze material, but only (1) resulted in almost octahedral crystals with well-defined faces.

$AgFAuF_4$. In the DRILAB, $AgFAsF_6$ (453 mg, 1.43 mmole) and $KAuF_4$ (402 mg, 1.29 mmole) were loaded into an FEP T-reactor fitted with two $\frac{3}{8}$-in.-o.d. FEP tubes and a Teflon valve. The reactor was pumped down in a dynamic vacuum (better than 0.05 Torr) and anhydrous HF (4 ml) was condensed onto the solid mixture. On warming to room temperature an insoluble green precipitate formed, the supernatant solution being colorless. The reactor was then pressurized with F_2 to 2 atm. No F_2 uptake was observed over several hours. The insoluble green product was washed free of $KAsF_6$ and excess $AgFAsF_6$ by decantation and back distillation of the AHF, this being repeated 10 times. X-ray powder photographs of the green material were indexed on the basis of a $CuFAuF_4$ type cell (7) as given in Table I.

$AgFAsF_6$ from excess AsF_5: In the DRILAB, AgF (1301 mg, 10.25 mmole) was loaded into a $\frac{1}{2}$-in.-o.d. FEP tube fitted with a Teflon valve. AHF (6 ml) was condensed under vacuum onto the AgF and this gave a colorless solution at room temperature. AsF_5 was allowed to dissolve in the solution and immediately produced a colorless precipitate of $AgAsF_6$. When no further AsF_5 uptake was observed at 1.5 atm, the AsF_5 supply was closed and the reactor was pressurized with F_2 to 2 atm. The mixture was vigorously agitated and uptake of F_2 was observed, the HF solution simultaneously becoming blue. After 24 hr F_2 uptake had ceased and a deep, royal-blue solution free of solid remained. The excess F_2, AsF_5, and HF were removed at room temperature in a dynamic vacuum to leave a dark, blue-green solid. The solid (3160 mg, 10.01 mmole) was held under vacuum for another 2 hr with no color change. X-ray powder photographs showed $AgFAsF_6$ lines only. Variable temperature magnetic susceptibility measurements showed temperature-independent paramagnetism above 63 K with a small paramagnetic impurity evident at temperatures below 63 K. No field dependence was observed from 6 to 280 K on switching from a 5- to a 40-kG field. The data are shown as A in Fig. 1.

$AgFAsF_6$ from stoichiometric AsF_5 addition. Several preparations were carried out in the following way. In the DRILAB, AgF (usually ~300 mg, 2.4 mmole) was loaded into an FEP T-reactor fitted with a Teflon valve. When the AHF (3 ml) which had been transferred in a dynamic vacuum was warmed to room temperature, a small amount of dark, insoluble material (perhaps AgF_2 from the fluorine used to passivate the reactor) precipitated out of the colorless solution. The solution was decanted into the free leg of the T and AsF_5 was admitted as above. On complete conversion of AgF to $AgAsF_6$ as judged by no further uptake of AsF_5, the AHF and any excess AsF_5 were removed in a dynamic vacuum, which was maintained for 3 hr. The colorless solid, $AgAsF_6$, that remained was washed twice with AHF (4 ml) by decantation to remove any unreacted AgF. This washed $AgAsF_6$ in AHF (4 ml) was pressurized with F_2 to 2 atm and the mixture was agitated. A deep blue solid formed as F_2 was taken up. F_2 uptake ceased after 8 hr. Removal of F_2 and AHF

TABLE I

X-RAY POWDER DATA FOR $AgFAuF_4$(Cu$K\alpha$, Ni FILTER)[a]

			$1/d^2 \times 10^4$		I/I_0					$1/d^2 \times 10^4$		I/I_0	
h	k	l	obsd	calcd	calcd[b]	obsd	h	k	l	obsd	calcd	calcd[b]	obsd
1	0	0	293	296	90	w		imp		2477	—	—	vvw
0	1	0	479	483	75	w		imp		2565	—	—	vvw
0	0	1	725	730	1000	vs	3	0	0	—	2663	5	—
1	$\bar{1}$	0		730	906		0	1	$\bar{2}$	—	2692	<1	—
1	1	0	826	828	753	s	1	1	$\bar{2}$	2716	2710	206	m
0	1	$\bar{1}$	—	858	19	—	1	0	$\bar{2}$	—	2887	4	—
1	0	$\bar{1}$	—	862	52	—	3	0	$\bar{1}$	—	2903	10	—
	imp		939	—	—	vvw	0	0	2	2917	2918	119	s
1	1	$\bar{1}$	1038	1039	493	s	2	$\bar{2}$	0		2919	163	
2	0	0	1183	1184	414	s	3	$\bar{1}$	0	3000	2999	180	m
1	0	1		1189	44		2	2	$\bar{1}$	3020	3004	134	m
1	$\bar{1}$	1	1256	1268	231	m	2	1	1	3191	3176	2	m
	imp		1487	—	—	vvw	3	1	$\bar{1}$		3178	104	
0	1	1		1567	98		1	$\bar{1}$	2	3246	3265	82	m
2	$\bar{1}$	0	1578	1569	33	m,br	2	$\bar{2}$	1		3266	91	
2	0	$\bar{1}$		1586	138		3	1	0	3302	3293	112	m
1	$\bar{1}$	$\bar{1}$	1652	1650	280	m	2	2	0		3311	108	
2	1	0	—	1765	2	—	2	1	$\bar{2}$	—	3320	9	—
2	1	$\bar{1}$	—	1813	11	—	0	2	1	3376	3370	85	w
0	2	0	1947	1931	193	s,br	1	$\bar{2}$	$\bar{1}$	—	3405	5	—
0	2	$\bar{1}$		1952	155		0	2	$\bar{2}$	3442	3431	104	m,br
1	1	1	2080	2075	182	m	2	0	$\bar{2}$		3448	77	
1	$\bar{2}$	0	—	2129	<1	—	1	2	$\bar{2}$	—	3498	11	—
1	2	$\bar{1}$		2182	51		1	0	2	—	3541	<1	—
2	0	1	2233	2240	201	s,br	3	$\bar{1}$	$\bar{1}$	3585	3593	86	m,br
2	$\bar{1}$	1		2270	37		3	$\bar{1}$	1	3858	3864	92	m,br
1	$\bar{2}$	1		2313	5		3	0	1	—	3883	15	—
1	2	0	2329	2325	11	vvw	1	2	1	—	3928	5	—
2	$\bar{1}$	$\bar{1}$		2326	13		1	$\bar{2}$	2	—	3956	6	—

[a] Triclinic cell with $a_0 = 5.906(6)$, $b_0 = 4.769(5)$, $c_0 = 3.933(5)$ Å, $\alpha = 107.01(5)$, $\beta = 99.46(4)$, $\gamma = 90.75(4)°$, $V = 104.3$ Å^3.

[b] The calculated intensities are based on parameters given by B. G. Müller (*7*) for the structure of $CuFAuF_4$, with which $AgFAuF_4$ is evidently isostructural.

left a dark blue solid (usually 700 mg, 2.2 mmole $AgFAsF_6$). X-ray powder photographs of this material showed only lines for the $AgFAsF_6$ phase (*3*). The results of variable temperature magnetic susceptibility measurements varied somewhat from sample to sample and are shown in Fig. 1.

In sample B, the appearance of a small field dependence below 163 K signifies a small AgF_2 impurity (see Fig. 5 for the susceptibility temperature profile for a dilute AgF_2 sample). There is more of that impurity in sample C, but in both B and C a marked decrease in susceptibility occurs below 63 K. The susceptibility of the AgF_2 impurity and perhaps a paramagnetic impurity eventually offset this decrease in chi as the temperature falls.

$AgFAuF_6$. In the DRILAB, $KAuF_6$ (*8*) (683 mg, 1.95 mmole) and $AgFAsF_6$ (810 mg,

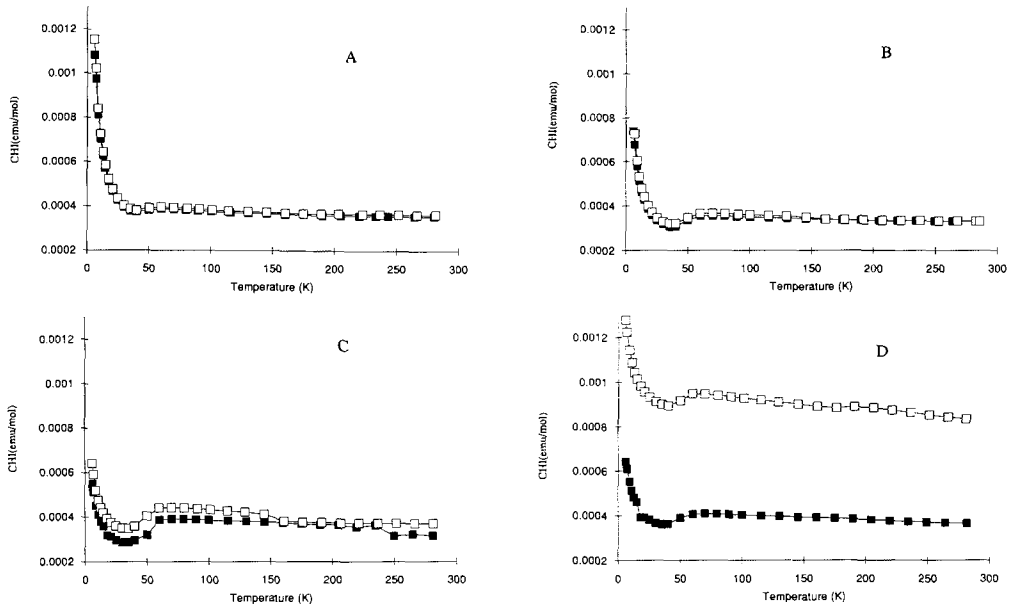

FIG. 1. Magnetic susceptibility data for $AgFAsF_6$ (A,B,C) and $AgFAuF_6$ (D). (□) 5 kG (■) 40 kG.

2.56 mmole) were loaded into one leg of an FEP T-reactor as described above. AHF (5 ml) was transferred into the reactor under static vacuum and on warming to room temperature provided a dark, green-blue precipitate, the supernatent solution being pale blue. The solid proved to be insoluble and was washed free of $KAsF_6$ and excess Ag $FAsF_6$ by decantation and back distillation of the AHF. After six washings the AHF over the solid was colorless. The AHF was removed in a dynamic vacuum, and the solid was dried under vacuum overnight. X-ray powder photographs of the solid showed it to be isomorphous with $AgFAsF_6$. The X-ray data are given in Table II. Variable temperature magnetic susceptibility measurements (see D, Fig. 1) showed behavior very similar to those for $AgFAsF_6$. Again a small AgF_2 impurity appears to be present; otherwise the susceptibility exhibits temperature-independent paramagnetism above 63 K, with a sharp drop just below that temperature. The apparent field dependence, even at temperatures above the Curie temperature for AgF_2 (163 K), is puzzling and could arise from a ferromagnetic contaminent.

$Ag(AuF_4)_2$. In the DRILAB, $AgFAsF_6$ and $KAuF_4$ (1 : 2) were loaded into separate legs of a Teflon T-reactor, described above. AHF (4 ml) was condensed into each leg of the reactor under static vacuum, resulting in yellow and blue solutions of $KAuF_4$ and $AgFAsF_6$, respectively. Pouring the $KAuF_4$ solution onto the $AgFAsF_6$ solution produced an olive-green precipitate, the supernatent solution being yellow. The reactor was pressurized with 2 atm BF_3 until the supernatent solution became colorless. The light green precipitate was washed 10 times by decantation and back distillation of the AHF to remove $KAsF_6$ and KBF_4 side products. AHF was removed and the light green solid was dried in a dynamic vacuum overnight. X-ray powder photographs showed a new phase similar to $Ag(AgF_4)_2$ (*4*). No lines attributable to $AgFAuF_4$ or AuF_3 were ob-

TABLE II

X-RAY POWDER DATA FOR $AgFAuF_6$($CuK\alpha$, Ni FILTER)[a]

			$1/d^2 \times 10^4$		I/I_0					$1/d^2 \times 10^4$		I/I_0	
h	k	l	obsd	calcd	calcd[b]	obsd	h	k	l	obsd	calcd	calcd[b]	obsd
1	0	1	268	270	119	w	1	2	3	1854	1830	27	w
0	1	1	286	293	41	w	3	1	1		1851	63	
0	0	2	—	389	8	—	0	3	1	1857	1855	12	m
	imp		425	—	—	vw	2	2	2		1863	23	
1	1	1	463	466	1000	vs	1	1	4	—	1925	8	—
1	0	2	562	562	263	m	3	0	2	—	1947	0.2	—
	imp		665	—	—	w	1	3	1	2045	2028	54	w,br
2	0	0	689	692	131	w,br	3	1	2	2142	2143	52	w,br
1	1	2	—	758	19	—	2	0	4	—	2250	0.1	—
0	2	0	782	781	381	s,br	1	3	2		2320	0.1	vvw
2	0	1		790	193		0	2	4	2321	2338	24	
2	1	0	—	888	0.2	—	2	2	3		2349	1	
2	1	1	976	985	20	vw	3	0	3		2434	0.1	
1	0	3	—	1049	4	—	3	2	1	2451	2437	41	w
1	2	1	—	1052	29	—	2	1	4		2445	32	
0	1	3	1070	1071	391	s	2	3	0		2450	2	
2	0	2		1082	64		1	2	4	2513	2511	99	w
0	2	2	—	1170	1.5	—	2	3	1	—	2547	11	—
1	1	3	1250	1244	56	vvw	1	0	5	—	2606	1	—
2	1	2	1287	1277	213	m	0	1	5	—	2628	0.5	—
1	2	2	1350	1344	173	m	3	1	3	—	2629	9.5	—
2	2	0	1473	1474	41	vw,br	0	3	3	2636	2633	151	m,br
0	0	4	—	1557	17	—	3	2	2	—	2728	12	—
2	0	3	1571	1568	0.5	wb	4	0	0	—	2770	3	—
2	2	1		1571	59		1	1	5	—	2801	22	—
3	0	1	1653	1655	35	w	1	3	3	—	2806	22	—
1	0	4	—	1730	18	—	2	3	2	2826	2839	103	m
2	1	3	1774	1764	92	w	4	0	1	2852	2867	13	w
							4	1	0	2963	2965	29	vw

[a] Orthorhombic unit cell with $a_0 = 7.600(4)$; $b_0 = 7.156(4)$; $c_0 = 10.137(5)$ Å; $V = 551.3$ Å^3. Probable space group *Pnma*.

[b] The calculated intensities are based on parameters given by Gantar *et al.* (*3*) for the structure of $AgFAsF_6$, with which $AgFAuF_6$ is evidently isostructural.

served. Variable temperature magnetic susceptibility measurements from 6 to 280 K at 5 and 40 kG obeyed the Curie–Weiss law for a dilute one-electron paramagnet with $\mu_{eff} = 1.82$ B.M. and $\Theta = -2°$ (Fig. 2).

Single-crystal X-ray structures for Ag FBF$_4$(violet) and AgFBF$_4$(bronze). A structure determination was carried out on both the needle form violet crystals of $AgFBF_4$ and the roughly octahedral-morphology crystals of bronze luster. The crystal data for both crystals are given in Table III; the positional and thermal parameters are compared in Table IV. Interatomic distances and angles are compared in Table V. No significant differences were detected in the two forms.

AgFAsF$_6$ single-crystal structure. Crystals of $AgFAsF_6$ were prepared as previously described from the interaction of

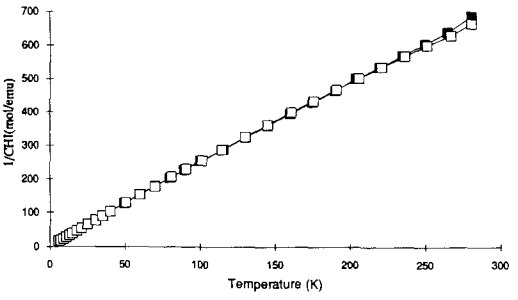

FIG. 2. Curie–Weiss plot for $Ag(II)Au(III)_2F_8$: (□) 5 kG; (■) 40 kG.

AgF_3 with AsF_5 in AHF (*4*). X-ray diffraction data were obtained at 186 K; the structure was solved and refined in the noncentrosymmetric space group $Pn2_1a$ (nonstandard setting of $Pna2_1$). Besides the well known distortions due to matrix singularities when a centrosymmetric structure is refined in a noncentrosymmetric space group, the structure was essentially the same as that described by Gantar *et al.* (*3*). Therefore the structure was finally refined in the centrosymmetric space group *Pnma*. Crystallographic data are given in Table VI, refined parameters in Table VII, and interatomic distances and angles in Table VIII.

Results and Discussion

The single-crystal structure of $AgFBF_4$ was successfully refined in space group $P4/n$. The earlier supposition (*1*) of a linear $(Ag–F)_n^{n+}$ chain, based on the tetragonal unit cell and tentative space group assignment,

TABLE III

CRYSTAL DATA AND DETAILS OF THE STRUCTURE REFINEMENT OF A VIOLET AND A BRONZE CRYSTAL OF $AgFBF_4$

	Violet	Bronze
Formula, mol wt	$AgBF_5$, 213.67 a.u.	
Temperature	293 K	
a_0	6.7000(3) Å	6.6995(14) Å
c_0	4.0113(2) Å	4.0116(13) Å
V	180.07(1) Å^3	180.05(7) Å^3
Z	2	
Space group	$P4/n$ (No. 85)	
$d_{calc.}$	3.940 g · cm^{-3}	
Crystal size	0.08 · 0.13 · 0.35 mm^3	0.17 · 0.17 · 0.17 mm^3
Wavelength (Mo$K\alpha$)	0.71069 Å	
μ	55.33 cm^{-1}	
Diffractometer	Enraf-Nonius CAD4, graphite monochromator	
Scan range	$3 < 2\Theta < 76°$; $\pm h$, $\pm k$, l	$6 < 2\Theta < 62°$; $\pm h$, k, l
Scan angle (deg)	1.1° + 0.35 · tan Θ; ω/Θ-scan	1.4 + 0.35 · tan Θ; ω/Θ-scan
Scan speed	variable, t_{max} = 80 sec	t_{max} = 90 sec
Data collected	2166	742
Independent	494; R_{int} = 0.026	288; R_{int} = 0.037
Absorption correction	ψ-scans, $\Delta\psi$ = 10°, 8hkl	4 hkl
Structure solution	By packing considerations from powder data (*1*)	
Refinement	Full matrix least squares, 17 parameters	
Weighting scheme	$1/\sigma^2$	
Extinction correction	$F_{corr} = F_{obs} \cdot (1 + g \cdot I)$, $g = 1.60 \times 10^{-5}$	None
R	0.0193	0.0230
wR	0.0250	0.0260
Goodness-of-fit	1.104	0.594

TABLE IV

POSITIONAL AND THERMAL PARAMETERS FOR VIOLET (UPPER SET) AND BRONZE (LOWER SET) $AgFBF_4$

	x	y	z	$U(1,1)$	$U(2,2)$	$U(3,3)$	$U(1,2)$	$U(1,3)$	$U(2,3)$
Ag	0.25	0.25	0.19212(7)	0.01496(6)	U(1,1)	0.00654(9)	0	0	0
	0.25	0.25	0.19236(10)	0.01922(9)	U(1,1)	0.00770(14)	0	0	0
F1	0.25	0.25	0.6930(7)	0.0341(9)	U(1,1)	0.009(1)	0	0	0
	0.25	0.25	0.6934(9)	0.0370(13)	U(1,1)	0.007(1)	0	0	0
B	0.25	0.75	0	0.021(1)	U(1,1)	0.017(2)	0	0	0
	0.25	0.75	0	0.025(2)	U(1,1)	0.023(3)	0	0	0
F2	0.3136(3)	0.5919(2)	0.1988(5)	0.047(1)	0.0206(6)	0.0315(8)	0.0031(7)	−0.0065(8)	0.0013(7)
	0.3136(5)	0.5914(4)	0.1984(6)	0.051(1)	0.0240(9)	0.0290(10)	0.0034(9)	−0.0043(11)	0.0014(9)

was confirmed. The structure of the roughly octahedral crystals of bronze luster, grown from solutions containing AgF, proved to be essentially the same as that derived from a violet crystal grown in the absence of AgF. The two structures are compared in Tables III–V.

The extended structure of $AgFBF_4$ is illustrated in Fig. 3. Four columns of linearly close-packed BF_4^- are seen to surround each linear $(Ag–F)_n^{n+}$ chain, and vice versa. Each Ag(II) atom is square-coordinated by four F ligands of the anions, each from one of the four surrounding BF_4^-, and is almost in the same plane as these four F ligands. Interaction of the almost ideally tetrahedral BF_4^- with four nearest-neighbor Ag(II) species, via the F ligands, results in an alternation of the Ag(II) z parameters in the four surrounding $(Ag–F)_n^{n+}$ columns, these z parameters being in step with those of the F ligands of an anion. As illustrated in Fig. 4, the Ag · · · F interatomic distances between cation and nearest anion ligands are 2.330(2) Å. These are consistent with interionic contacts. The Ag–F distances within the chain, on the other hand, are short and must represent appreciable overlap of the valence-shell orbitals of the Ag(II) (e.g., $4d_{z^2}$) and the F (e.g., $2p_z$). Evidently the antibonding influence of the Ag(II) d^9 configuration is minimal in the cationic chain; therefore, the unique, half-filled d orbital is designated d_{z^2}. The crystal orbitals for the cationic chain must be dominated by the contributions from $4d_{z^2}$ of Ag(II) and $2p_z$ of F. Since this signifies a half-filled conduction band, a Peierls distortion is anticipated. In this room-temperature structure, however, no such distortion is manifest. Indeed, each

TABLE V

INTERATOMIC DISTANCES (Å) AND ANGLES (°) FOR VIOLET (UPPER SET) AND BRONZE (LOWER SET) $AgFBF_4$

	Distances			Angles		
a	Ag–F1	2.002(3)		F1–Ag–F1′	180	
		2.002(4)			180	
b	Ag–F1′	2.009(3)	4 × F1–Ag–F2	90.66(5)	4 × F1′–Ag–F2	89.34(50
		2.010(4)		90.60(6)		89.40(6)
c	4 × Ag–F2	2.330(2)	4 × F2–Ag–F2	89.992(1)	2 × F2–Ag–F2	178.68(9)
		2.327(3)		89.994(1)		178.80(13)
d	4 × B–F2	1.393(2)	4 × F2–B–F2	109.14(8)	2 × F2–B–F2	110.1(2)
		1.394(3)		109.02(10)		110.4(2)

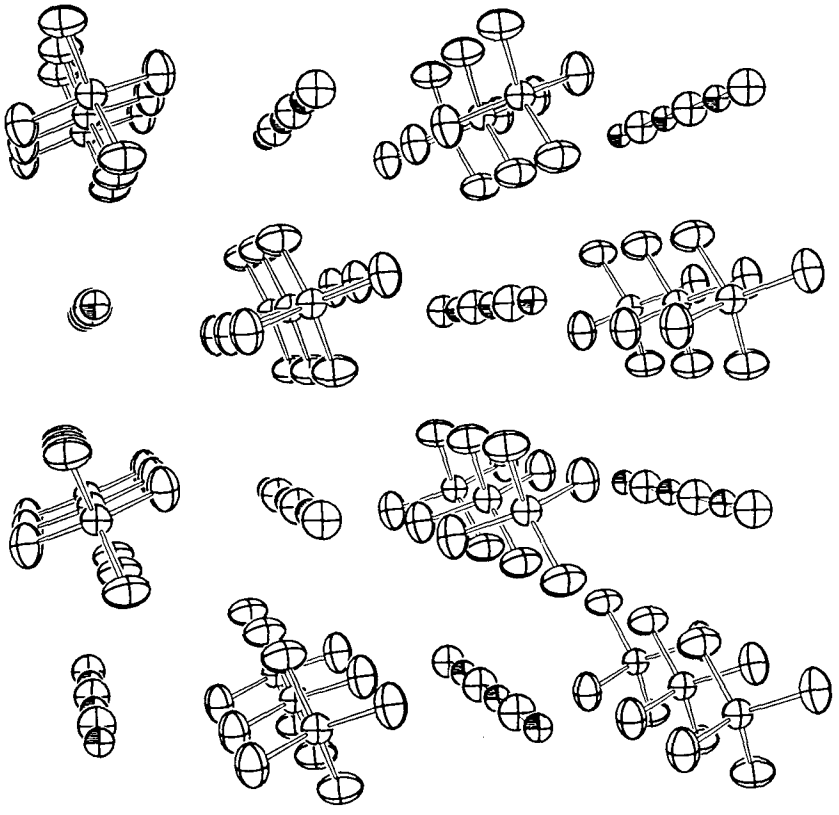

FIG. 3. The $AgFBF_4$ extended structure (50% probability ellipsoids).

Ag(II) is in a highly polar electric field, since all four nearest boron atoms of each Ag(II) are either above or below it with respect to the chain direction. Nevertheless, the two intrachain Ag–F distances are remarkably close at 2.002(3) and 2.009(3) Å. (The difference can be readily reconciled by the way in which the anion packing dictates that the four additional anion F ligands directed toward each Ag(II) are not in exactly the same plane as it.)

The Peierls distortion to be expected for the $(Ag–F)_n^{n+}$ chain is an alternation of linear, symmetrical $(F–Ag–F)^+$ species and Ag^+, interatomic distances in the chain becoming short about the Ag(III) and long about the Ag(I). But the polar field about each Ag(II) in the chain must frustrate the required centrosymmetric F ligand displacement about each Ag atom. It is perhaps for this reason that the magnetic susceptibility data show no signs of a Peierls transition.

The ease of reduction of $AgFBF_4$ and the necessity of prefluorinating all containers have resulted in some contamination of samples used in the magnetic susceptibility measurements. All samples examined have, however, been characterized by approximate temperature independence of the susceptibility. The most common identifiable impurity has been AgF_2. This is ferromagnetic and is characterized (*9*) by a Curie temperature of 163 K. Roughly 1.5% AgF_2 impurity affects the susceptibility data displayed in Fig. 5. The field dependence of a dilute sample of AgF_2 (mixed with 85% CaF_2) is illustrated on the same plot; this simultaneously confirms the nature of the field-dependent impurity present in the $AgFBF_4$, and the temperature-indepen-

TABLE VI

CRYSTAL DATA AND DETAILS OF THE STRUCTURE REFINEMENT OF $AgFAsF_6$

Formula, mol wt	$AgAsF_7$, 315.78 a.u.
Temperature	186 K
a_0	7.575(2) Å
b_0	6.970(1) Å
c_0	9.792(2) Å
V	517.0(3) Å^3
Z	4
Space group	*Pnma* (No. 62)
$d_{calc.}$	4.057 g · cm^{-1}
Crystal size	0.18 · 0.25 · 0.76 mm^3
Wavelength (Mo$K\alpha$)	0.71069 Å
μ	102.77 cm^{-1}
Diffractometer	Enraf-Nonius CAD4, graphite monochromator
Scan range	$3 < 2\Theta < 60°$; h, $\pm k$, l
Scan angle	0.9° + 0.35 · tan Θ
Scan speed	6.67 °/min
Data collected	1697
Independent	808; R_{int} = 0.032 for 727 with $I > 3 \cdot \sigma(I)$
Absorption correction	ψ-scans, 4 hkl, $\Delta\psi$ = 10°, T_{max} = 0.99, T_{min} = 0.64
Structure solution	Ag and As atoms with Patterson method
Refinement	Full matrix least squares, 50 parameters
Weighting scheme	$1/\sigma^2$
Extinction correction	$F_{corr} = F_{obs} \cdot (1 + g \cdot I)$, g = 1.194 × 10^{-6}
R, R'	0.0206, 0.0264
wR	0.0264
Goodness-of-fit	1.385

dence of the susceptibility of the latter in the temperature range 6 to 280 K. The magnitude of the molar susceptibility (182(3) × 10^{-6} emu mole^{-1}) is similar to that of $AgFAsF_6$, in its temperature-independent range (see below), and is that anticipated for a partially filled band, obedient to Fermi–Dirac statistics (*10*). Therefore it is likely that the crystals of $AgFBF_4$ will be good electronic conductors in the c axis direction. Certainly the crystals exhibit high reflectance (bronze-luster) of plane-polarized visible light when the c axis is in the plane of the electric vector. With the electric vector of the light perpendicular to the c axis a crystal is transparent and lilac. The crystal is opaque to light with the electric vector parallel to c. These optical properties are common to one-dimensional metals (*11*).

A single crystal of $AgFAsF_6$ prepared (*4*) from interaction of AgF_3 with AsF_5 in AHF (Eq. (1)) was cooled (to 166 K) to check that the structural features reported by Gantar *et al.* (*3*) were still valid at the lower temperature. Of particular interest was the insignificant difference in the two distances of the cationic chain, Ag–F = 2.004(5) and 1.995(5) Å, reported by them. The structure was initially deliberately refined in the lower symmetry space group $Pn2_1a$, but this model proved to contain, in effect, the additional mirror plane of *Pnma*. Although there are (because of the much lower temperature) small differences in the unit cell and positional parameters from those given by Gantar *et al.* (*3*), there are no important structural differences. In particular the intrachain Ag–F distances (see Table VIII) are no less equal than in the room-temperature structure. Unfortunately it has not yet been possible to carry out the structure determination below 63 K, where the magnetic susceptibility data indicate the possibility of a Peierls transition.

As in the case of the $AgFBF_4$ magnetic data, impurities had a varying and a sometimes profound impact on the measured

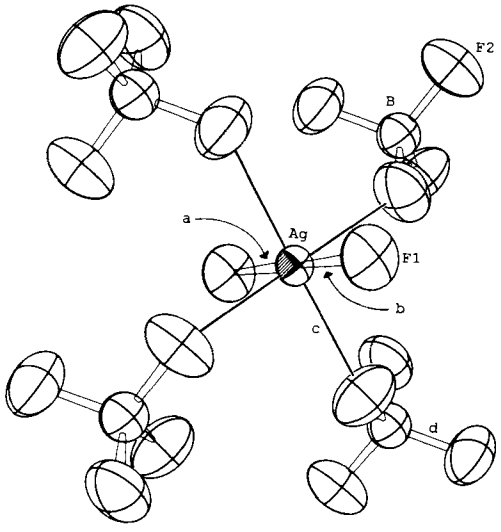

FIG. 4. The tetragonally distorted octahedral F environment of the Ag(II) in $AgFBF_4$ (90% probability ellipsoids). Interatomic distances correspond to those in Table V.

TABLE VII

POSITIONAL AND THERMAL PARAMETERS FOR $AgFAsF_6$ AT 186 K

	x	y	z	$U(1,1)$	$U(2,2)$	$U(3,3)$	$U(1,2)$	$U(1,3)$	$U(2,3)$
Ag	0.13239(1)	0.25	0.24283(1)	0.0076(1)	0.0123(1)	0.0125(1)	0	−0.00104(9)	0
As	0.30012(1)	0.25	0.56159(1)	0.0142(2)	0.0138(1)	0.0108(2)	0	0.0002(1)	0
F1	0.3850(3)	0.25	0.1855(3)	0.007(1)	0.029(1)	0.020(1)	0	−0.0004(8)	0
F2	0.5058(4)	0.25	0.4845(3)	0.015(1)	0.032(1)	0.020(1)	0	0.003(1)	0
F3	0.0999(4)	0.25	0.6351(3)	0.022(1)	0.063(2)	0.032(1)	0	0.011(1)	0
F4	0.2329(3)	0.0781(3)	0.4450(2)	0.0328(9)	0.0200(8)	0.0200(7)	−0.0059(8)	−0.0088(7)	−0.0037(7)
F5	0.3747(2)	0.0752(3)	0.6708(2)	0.039(1)	0.0148(7)	0.0190(7)	−0.0024(7)	−0.0081(7)	0.0048(7)

magnetic susceptibility, especially at low temperatures. Three separate sets of data for $AgFAsF_6$ (from different preparations) are compared in Fig. 1. As in the $AgFBF_4$ (Fig. 5) it is clear that small AgF_2 impurities are responsible for the field-dependent features below 163 K (see data from samples B and C). In addition, there is probably a small but unidentified paramagnetic impurity. In all cases, however, the magnetic susceptibility of $AgFAsF_6$ appears to be essentially temperature-independent in the range 63 to 280 K. The sharp drop in susceptibility at 63 K is probably indicative of a Peierls distortion, but the paramagnetic and ferromagnetic impurities hide the anticipated diamagnetism consequent upon such a transition.

The X-ray powder data for $AgFAuF_6$ (see Table II) show that this salt is isostructural with $AgFAsF_6$. The intrachain distances and the chain kinking must be very similar to those observed in $AgFAsF_6$. Perhaps the kinking of the cationic chain in these structures (Ag–F–Ag ~143°) results in lower elastic forces than those pertaining in the linear $AgFBF_4$ chain, this accounting for the Peierls distortion being accommodated in the kinked cation chain and not in the straight. It is, however, remarkable that the drop in susceptibility, indicative of a Peierls

TABLE VIII

INTERATOMIC DISTANCES (Å) AND ANGLES (°) FOR $AgFAsF_6$ AT 186K (SEE REF. (3) FOR APPROPRIATE FIGURE)

Distances		Angles			
Ag–F1^{i}	1.994(2)	F1–Ag–F1^{i}	175.82(10)	Ag–F1–Ag^{v}	143.12(4)
Ag–F1	2.001(2)	F1–Ag–F2^{i}	96.95(10)	F1^{i}–Ag–F2^{i}	87.24(10)
Ag–F2^{i}	2.424(3)	F1–Ag–F4	85.92(8)	F1^{i}–Ag–F4^{iv}	90.44(8)
Ag–F4	2.436(2)	F1–Ag–F5^{ii}	86.45(5)	F1^{i}–Ag–F5^{ii}	94.76(5)
Ag–F5^{ii}	2.375(2)	F2^{i}–Ag–F4	150.46(4)	F2^{i}–Ag–F5^{ii}	73.62(4)
As–F2	1.731(3)	F4–Ag–F5^{ii}	135.90(6)	F4^{iv}–Ag–F5^{ii}	77.24(6)
As–F3	1.678(3)	F4–Ag–F4^{iv}	58.93(6)	F5^{iii}–Ag–F5^{ii}	145.31(6)
As–F4	1.732(2)	F4^{iv}–As–F5^{iv}	90.92(9)	F4^{iv}–As–F5	176.92(9)
As–F5	1.717(2)	F4^{iv}–As–F4	87.59(9)	F5–As–F5^{iv}	90.44(9)
		F2–As–F3	179.54(14)	F3–As–F4	90.97(10)
		F2–As–F4	88.69(9)	F3–As–F5	91.75(10)
		F2–As–F5	88.58(9)	Ag^{v}–F2–As	139.14(14)
		Ag–F4–As	106.69(9)	Ag^{ii}–F5–As	148.78(10)

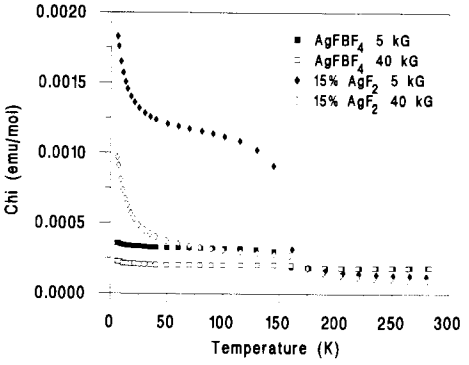

FIG. 5. Magnetic susceptibility data of $AgFBF_4$, at two field strengths, compared with dilute AgF_2 (15% AgF_2, 85% CaF_2). AgF_2 is ferromagnetic with a Curie temperature of 163 K (*9*).

transition in $AgFAuF_6$ (see Fig. 1), occurs at the same temperature (63 K) as in $AgFAsF_6$.

It remains to be seen if the susceptibility of $AgFAuF_4$ (which is isostructural (*7*) with $CuFAuF_4$ and must therefore have a straight cation chain) exhibits a Peierls transition. It is difficult to obtain it free of either AgF_2 or $Ag(AuF_4)_2$. The latter salt is, however, preparable in high purity, and as may be seen from the Curie law behavior of its susceptibility in Fig. 2, it is a dilute paramagnet. Here the d^9 Ag(II) species must be well separated from one another by the diamagnetic, square AuF_4^- ions (d^8). Although the structure is not yet known, it probably will have coordination features for the Ag(II) akin to those in $Ag(SbF_6)_2$ as described by Gantar *et al.* (*12*).

It remains to be seen how well the $(Ag–F)_n^{n+}$ chains in these salts conduct electricity and, especially, how the kinked chains compare with the straight ones in this regard.

Acknowledgments

The work was supported by the Director, Office of Energy Research, Office of Basic Energy Sciences, by the Chemical Science Division of the U.S. Department of Energy under Contract DE-AC03-67SF00098. Additional support was provided by the U.S.–Yugoslav Joint Fund for Scientific and Technological Cooperation, in association with the National Science Foundation under Grant JF947. The authors also thank Dr. G. V. Shalimoff for assistance with susceptibility measurements and Dr. F. Hollander for expert help in assessing the correct space group for the $AgFAsF_6$ structure. One of us (H. B.) also gratefully acknowledges the Alexander von Humboldt Foundation for a Feodor Lynen Fellowship.

References

1. B. ŽEMVA, R. HAGIWARA, W. J. CASTEEL, JR., K. LUTAR, A. JESIH, AND N. BARTLETT, *J. Am. Chem. Soc.* **112,** 4846 (1990).
2. W. J. CASTEEL, JR., R. HAGIWARA, AND N. BARTLETT, *to be published.*
3. D. GANTAR, B. FRLEC, D. R. RUSSELL, AND J. H. HOLLOWAY, *Acta Crystallogr. Sect. C. Cryst. Struct. Commun.* **43,** 618 (1987).
4. B. ŽEMVA, K. LUTAR, A. JESIH, W. J. CASTEEL, JR., A. P. WILKINSON, D. E. COX, R. B. VON DREELE, H. BORRMANN, AND N. BARTLETT, *J. Am. Chem. Soc.,* in press (1991).
5. "Matheson Gas Data Book," 4th ed., p. 273, Hearst, New York (1966).
6. D. W. A. SHARP AND A. G. SHARPE, *J. Chem. Soc.,* 1855 (1956).
7. B. G. MÜLLER, *Angew. Chem. Int. Ed. Engl.* **26,** 688 (1987).
8. N. BARTLETT AND K. LEARY, *Rev. Chim. Minér.* **13,** 82 (1976).
9. E. GRUNER AND W. KLEMM, *Naturwissenschaften* **25,** 59 (1937); P. CHARPIN, A. J. DIANOUX, H. MARQUET-ELLIS, AND NGUYEN-NGHI, *C.R. Acad. Sci. Paris* **264** 1108 (1967).
10. CHARLES KITTEL, "Introduction to Solid State Physics," p. 413, Wiley, New York (1986).
11. A. D. YOFFE, *Chem. Soc. Rev.* **5**(1), 51 (1976).
12. D. GANTAR, I. LEBAN, B. FRLEC, AND J. H. HOLLOWAY, *J. Chem. Soc. Dalton Trans.,* 2379 (1987).